A meshless method for the stable solution of singular inverse problems for two-dimensional Helmholtz-type equations

Liviu Marin *

Institute of Solid Mechanics, Romanian Academy, 15 Constantin Mille, Sector 1, P.O. Box 1-863, 010141 Bucharest, Romania

ARTICLE INFO

ABSTRACT

We investigate a meshless method for the stable and accurate solution of inverse problems associated with two-dimensional Helmholtz-type equations in the presence of boundary singularities. The governing equation and boundary conditions are discretized by the method of fundamental solutions (MFS). The existence of boundary singularities affects adversely the accuracy and convergence of standard numerical methods. Solutions to such problems and/or their corresponding derivatives may have unbounded values in the vicinity of the singularity. Moreover, when dealing with inverse problems, the stability of solutions is a key issue and this is usually taken into account by employing a regularization method. These difficulties are overcome by combining the Tikhonov regularization method (TRM) with the subtraction from the original MFS solution of the corresponding singular solutions, without an appreciable increase in the computational effort and at the same time keeping the same MFS discretization. Three examples for both the Helmholtz and the modified Helmholtz equations are carefully investigated.

1. Introduction

Helmholtz-type equations are often used to describe the acoustic cavity problem [1], the heat conduction in fins [2], the vibration of a structure [3], the radiation wave [4] and the scattering of a wave [5]. In many engineering problems governed by Helmholtz-type equations, boundary singularities arise when there are sharp re-entrant corners in the boundary, the boundary conditions change abruptly, or there are discontinuities in the material properties. It is well known that these situations give rise to singularities of various types and, as a consequence, the solutions to such problems and/or their corresponding derivatives may have unbounded values in the vicinity of the singularity. Singularities are known to affect adversely the accuracy and convergence of standard numerical methods, such as finite element (FEM), boundary element (BEM), finite-difference (FDM), spectral and meshless/meshfree methods. If, however, the form of the singularity is taken into account and is properly incorporated into the numerical scheme then a more effective method may be constructed.

There are important studies regarding the numerical treatment of singularities in Helmholtz-type equations, see e.g. [3–11]. Chen et al. [3] analysed time-harmonic waves in a membrane which contains one or more fixed edge stringers or cracks by using the

dual BEM. Huang et al. [4] investigated the electromagnetic field due to a line source radiating in the presence of a two-dimensional composite wedge made of a number of conducting and dielectric materials by employing the Fourier transform path integral method. A hybrid asymptotic/FEM for computing the acoustic field radiated or scattered by acoustically large objects was developed by Barbone et al. [5]. The method of the auxiliary mapping and the p-version of the FEM were employed by Cai et al. [6] and Lucas and Oh [7] to remove the pollution effect caused by singularities in the Helmholtz equation. Wu and Han [8] solved singular boundary value problems for both Laplace and Helmholtz-type equations by using the FEM and introducing a sequence of approximations to the boundary conditions at an artificial boundary. Xu and Chen [9] used the FDM and higher-order discretized boundary conditions at the edges of perfectly conducting wedges for TE waves to retrieve accurately the field behaviour near a sharp edge. The treatment of singularities in both isotropic and anisotropic two-dimensional Helmholtz-type equations was investigated by Marin et al. [10], who modified the standard BEM to account for the presence of singularities. For an excellent survey on the treatment of singularities in elliptic boundary value problems, we refer the reader to Li and Lu [11] and the references therein.

The method of fundamental solutions (MFS) is a meshless/meshfree boundary collocation method which is applicable to boundary value problems for which a fundamental solution of the operator in the governing equation is known. In spite of this restriction, it has, in recent years, become very popular primarily

* Tel./fax: +40 (0) 21 312 6736.
  E-mail addresses: marin.liviu@gmail.com, liviu@imsar.bu.edu.ro.

because of the ease with which it can be implemented, in particular for problems in complex geometries. Since its introduction as a numerical method by Mathon and Johnston [12], it has been successfully applied to a large variety of physical problems, an account of which may be found in the survey papers [13–16]. Recently, the MFS has been successfully applied to solving inverse problems associated with the heat equation [17,18], linear elasticity [19,20], steady-state heat conduction in functionally graded materials [21], Helmholtz-type equations [22–24], and source reconstruction in steady-state heat conduction problems [25]. Numerous studies in the literature have been devoted to the application, in a stable manner, of the MFS to singular problems, see [26–31]. The standard MFS was modified in order to take into account the presence of boundary singularities in both the Laplace and the biharmonic equations by Karageorghis [26] and Poullikkas et al. [27], respectively. Karageorghis et al. [28] adapted the MFS formulation to obtaining stable solutions in linear elastic fracture mechanics problems involving the opening mode (mode I). Later, Berger et al. [29] extended the method developed in [28] to problems involving not only the opening mode, but the forward shear mode (mode II) as well, and also proposed another solution method based on a domain decomposition approach. Marin [30] applied the MFS, in conjunction with the removal of the associated singular functions and regularization methods, to the stable solution of both direct and inverse problems for the Laplace equation subject to noisy boundary data. Recently, this method was extended to solving, in a stable manner, direct problems for Helmholtz-type equations, see e.g. Marin [31].

The objective of this paper is to propose, implement and analyse the MFS for the accurate and stable solution of inverse problems associated with two-dimensional Helmholtz-type equations in the presence of boundary singularities. The existence of boundary singularities affect adversely the accuracy and convergence of standard numerical methods. Consequently, solutions to such problems and/or their corresponding derivatives, which are obtained by a straightforward inversion of the MFS system, may have unbounded values in the vicinity of the singularity. Moreover, when dealing with inverse problems subject to noisy data, the stability of solutions becomes a key issue and this is usually accounted for by employing regularization methods. These difficulties are overcome by combining the Tikhonov regularization method (TRM) with the subtraction from the original MFS solution of the corresponding singular solutions, i.e. using the so-called singularity subtraction technique (SST), see e.g. Portela et al. [32], without an appreciable increase in the computational effort and at the same time keeping the original MFS discretization. The proposed modified MFS is then implemented for inverse problems associated with both the Helmholtz and the modified Helmholtz equations in two-dimensional domains with an edge crack or a V-notch, as well as an L-shaped domain.

2. Mathematical formulation

We assume that the homogeneous Helmholtz-type equation is satisfied in the two-dimensional bounded domain Ω with a piecewise smooth boundary $\Gamma = \partial\Omega$, such that the potential solution and normal flux can be measured on $\Gamma_D \subsetneq \Gamma$ and $\Gamma_N \subsetneq \Gamma$, respectively, where $\Gamma_D \neq \emptyset$ and $\Gamma_N \neq \emptyset$. Moreover, both Dirichlet and Neumann data (i.e. Cauchy data) are available on a portion $\Gamma_C = \Gamma_D \cap \Gamma_N$ of the boundary Γ, where $\Gamma_C \neq \emptyset$, while neither the potential solution, nor the normal flux can be measured on $\Gamma \backslash (\Gamma_D \cup \Gamma_N) \neq \emptyset$ and they have to be determined. Hence the inverse problem considered recasts as:

$$\Delta u(\mathbf{x}) \pm k^2 u(\mathbf{x}) \equiv \frac{\partial^2 u(\mathbf{x})}{\partial x_1^2} + \frac{\partial^2 u(\mathbf{x})}{\partial x_2^2} \pm k^2 u(\mathbf{x}) = 0, \quad \mathbf{x} \in \Omega \tag{1.1}$$

$$u(\mathbf{x}) = \tilde{u}^{\varepsilon}(\mathbf{x}), \quad \mathbf{x} \in \Gamma_D \tag{1.2}$$

$$q(\mathbf{x}) \equiv \nabla u(\mathbf{x}) \cdot n(\mathbf{x}) = \tilde{q}^{\varepsilon}(\mathbf{x}), \quad \mathbf{x} \in \Gamma_N, \tag{1.3}$$

where $k \in \mathbb{R}$, the plus sign corresponds to the Helmholtz equation, while the minus sing is associated with the modified Helmholtz equation, and $\tilde{u}^{\varepsilon}|_{\Gamma_D}$ and $\tilde{q}^{\varepsilon}|_{\Gamma_N}$ are perturbed prescribed boundary potential solution and normal flux, respectively, given by

$$\tilde{u}^{\varepsilon}|_{\Gamma_D} = \tilde{u}|_{\Gamma_D} + \delta u, \quad \tilde{q}^{\varepsilon}|_{\Gamma_N} = \tilde{q}|_{\Gamma_N} + \delta q. \tag{2}$$

Here $\delta\tilde{u}$ and $\delta\tilde{q}$ are Gaussian random variables with mean zero and standard deviations $\sigma_u = \max_{\Gamma_D}|u| \times (p_u/100)$ and $\sigma_q = \max_{\Gamma_N}|q| \times (p_q/100)$, respectively, generated by the NAG subroutine G05DDF, and p_u and p_q are the percentages of additive noise included into the exact input data $u|_{\Gamma_D}$ and $q|_{\Gamma_N}$, respectively, in order to simulate the inherent measurement errors.

In addition, we also assume that the boundary Γ contains a singularity at the origin O, which may be caused by a change in the boundary conditions at the origin and/or a re-entrant corner at the origin. For the simplicity of the following explanations, we assume that the singularity point is located at the intersection of the Dirichlet, Γ_D, and Neumann, Γ_N, boundary parts, i.e. $\{O\} \subset \overline{\Gamma}_D \cap \overline{\Gamma}_N$, where $\Gamma_D \neq \emptyset$, $\Gamma_N \neq \emptyset$, $\Gamma_D \subset \Gamma$, $\Gamma_N \subset \Gamma$ and we denote by an overbar the closure of a set, see Fig. 1(a), although the method presented in this paper can easily be extended to other local configurations or boundary conditions.

It is well known that, even for two-dimensional domains with smooth boundaries, inverse problems are in general considerably more difficult to solve than direct problems since the solution does not satisfy the general conditions of well-posedness. More precisely, small measurement errors in the input data may result in very large errors in the solution, see e.g. Hadamard [33]. Moreover, the inverse problem under investigation (1.1)–(1.3) is considerably more severe than a regular inverse problem, as described above, since the additional singularity amplify the unstable character of the problem. Hence we cannot use a direct approach, such as the least-squares method (LSM), in order to solve the system of linear equations which arises from the discretization of the inverse boundary value problem (1.1)–(1.3).

3. Singular solutions for two-dimensional Helmholtz-type equations

In this section, some well-known results on the solution of the homogeneous two-dimensional Helmholtz-type equations are revised. For more details, we refer the reader to Marin et al. [10] and the references therein. For a fixed non-zero complex number κ the homogeneous Helmholtz-type equation in $\Omega \subset \mathbb{R}^2$ can be written as

$$\Delta u(\mathbf{x}) + \kappa^2 u(\mathbf{x}) = 0, \quad \mathbf{x} = (x_1, x_2) \in \Omega. \tag{3}$$

Note that the values $\kappa = k$ and $\kappa = ik$, where $k \in \mathbb{R}$, correspond to the real Helmholtz and modified Helmholtz equations, respectively. Let the polar coordinate system (r, θ) be defined in the usual way with respect to the Cartesian coordinates $(x_1, x_2) = (r\cos\theta, r\sin\theta)$. If we assume that the solution of Eq. (3) in the domain Ω can be written using the separation of variables with respect to the polar coordinates (r, θ), where $r > 0$, then the general solution of the Helmholtz-type Eq. (3) can be written as

$$u(r, \theta) = [\gamma_1 J_{\lambda}(\kappa r) + \gamma_2 N_{\lambda}(\kappa r)][a\cos(\lambda\theta) + b\sin(\lambda\theta)]. \tag{4}$$
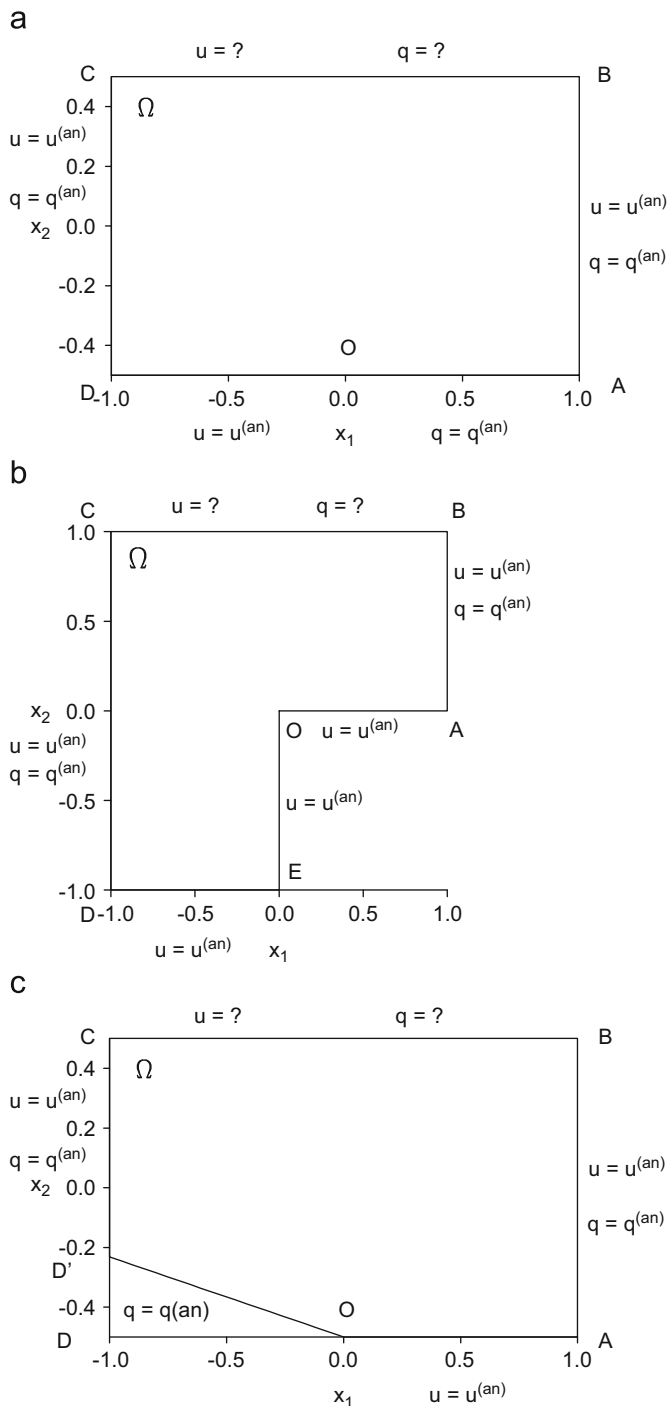
a

b

c

Fig. 1. Schematic diagram of the geometry and boundary conditions for the singular inverse problems investigated, namely: (a) Example 1: N–D singularity in a domain containing an edge crack OD with $\theta_1 = 0$ and $\theta_2 = \pi$, (b) Example 2: D–D singularity in an L-shaped domain with $\theta_1 = 0$ and $\theta_2 = 3\pi/2$, and (c) Example 3: D–N singularity in a domain containing a V-notch with $\theta_1 = 0$ and $\theta_2 = 11\pi/12$.

Here γ_1, γ_2, a and b are constants, whilst J_λ and N_λ are the Bessel functions of the first kind and the second kind, respectively.

Consider now that Ω is a two-dimensional isotropic wedge domain of interior angle, $\theta_2 - \theta_1$, with the tip at the origin, O, of the local polar coordinates system and determined by two straight edges of angles θ_1 and θ_2, given by $\Omega = \{\mathbf{x} \in \mathbb{R}^2 | 0 < r < R(\theta),$ $\theta_1 < \theta < \theta_2\}$, where $R(\theta)$ is either a bounded continuous function

or infinity. Moreover, we consider the boundary value problem given by Eq. (3) in Ω and homogeneous Neumann and/or Dirichlet boundary conditions prescribed on the wedge edges. On assuming $\mathrm{Re}\,\lambda \geq 0$ and taking into account the finite character of the potential solution, u, in a wedge tip neighbourhood, we obtain $\gamma_2 = 0$ in Eq. (4). Hence the basis function of singular functions to the aforementioned boundary value problem obtained from expression (4) can be written in the general form as

$$u^{(S)}(r,\theta) = J_\lambda(\kappa r)[a\cos(\lambda\theta) + b\sin(\lambda\theta)], \tag{5}$$

where a and b are the unknown singular coefficients, whilst λ is referred to as the singularity exponent or eigenvalue. The singularity exponent/eigenvalue, as well as the corresponding singular coefficients, are determined by the geometry and boundary conditions along the boundaries sharing the singular point.

The normal flux through a straight radial line defined by an angle θ and associated with the normal vector $\mathbf{n}(\theta) = (-\sin\theta, \cos\theta)$ is given by

$$q^{(S)}(r,\theta) = \frac{1}{r}\frac{\partial}{\partial\theta}u^{(S)}(r,\theta). \tag{6}$$

For the sake of convenience, the singular function, $u^{(S)}$, and normal flux, $q^{(S)}$, given by Eqs. (5) and (6), respectively, can be recast as

$$u^{(S)}(r,\theta) = J_\lambda(\kappa r)\{a\cos[\lambda(\theta - \theta_1)] + b\sin[\lambda(\theta - \theta_1)]\}, \tag{7}$$

$$q^{(S)}(r,\theta) = \frac{\lambda}{r}J_\lambda(\kappa r)\{-a\sin[\lambda(\theta - \theta_1)] + b\cos[\lambda(\theta - \theta_1)]\}. \tag{8}$$

Four configurations of homogeneous Neumann (N) and Dirichlet (D) boundary conditions at the wedge edges applied to expressions (7) and (8) are considered in this paper. On assuming the existence of a nontrivial solution of the resulting system of equations under the assumption $\mathrm{Re}\,\lambda \geq 0$, one obtains the general asymptotic expansions for the singular function of Helmholtz-type equations for a single wedge and corresponding to homogeneous Neumann and Dirichlet boundary conditions on the wedge edges, see also Marin et al. [10]:

Case I: N–N wedge

$$u^{(S)}(r,\theta) = \sum_{n=0}^{\infty} a_n u_n^{(NN)}(r,\theta) = \sum_{n=0}^{\infty} a_n J_{\lambda_n}(\kappa r)\cos[\lambda_n(\theta - \theta_1)],$$
$$\lambda_n = n\frac{\pi}{\theta_2 - \theta_1}, \quad n \geq 0. \tag{9}$$

Case II: N–D wedge

$$u^{(S)}(r,\theta) = \sum_{n=1}^{\infty} a_n u_n^{(ND)}(r,\theta) = \sum_{n=1}^{\infty} a_n J_{\lambda_n}(\kappa r)\cos[\lambda_n(\theta - \theta_1)],$$
$$\lambda_n = \left(n - \frac{1}{2}\right)\frac{\pi}{\theta_2 - \theta_1}, \quad n \geq 1. \tag{10}$$

Case III: D–D wedge

$$u^{(S)}(r,\theta) = \sum_{n=1}^{\infty} a_n u_n^{(DD)}(r,\theta) = \sum_{n=1}^{\infty} a_n J_{\lambda_n}(\kappa r)\sin[\lambda_n(\theta - \theta_1)],$$
$$\lambda_n = n\frac{\pi}{\theta_2 - \theta_1}, \quad n \geq 1. \tag{11}$$

Case IV: D–N wedge

$$u^{(S)}(r,\theta) = \sum_{n=1}^{\infty} a_n u_n^{(DN)}(r,\theta) = \sum_{n=1}^{\infty} a_n J_{\lambda_n}(\kappa r)\sin[\lambda_n(\theta - \theta_1)],$$
$$\lambda_n = \left(n - \frac{1}{2}\right)\frac{\pi}{\theta_2 - \theta_1}, \quad n \geq 1. \tag{12}$$

4. Singularity subtraction technique

In order to avoid the numerical difficulties arising from the presence of the singularity in the solution at O, it is convenient to modify the original problem before it is solved by the MFS. Due to the linearity of the Helmholtz and modified Helmholtz operators, as well as the boundary conditions, the superposition principle is valid and the potential solution, u, and normal flux, q, can be written as, see e.g. [10,30–32],

$$u(\mathbf{x}) = (u(\mathbf{x}) - u^{(S)}(\mathbf{x})) + u^{(S)}(\mathbf{x}) = u^{(R)}(\mathbf{x}) + u^{(S)}(\mathbf{x}),$$
$$\mathbf{x} \in \overline{\Omega} = \Omega \cup \Gamma, \tag{13}$$

$$q(\mathbf{x}) = (q(\mathbf{x}) - q^{(S)}(\mathbf{x})) + q^{(S)}(\mathbf{x}) = q^{(R)}(\mathbf{x}) + q^{(S)}(\mathbf{x}), \quad \mathbf{x} \in \Gamma, \tag{14}$$

where $u^{(S)}(\mathbf{x})$ is a particular singular potential solution of the original problem (1.1)–(1.3) which satisfies the corresponding homogeneous boundary conditions on the parts of the boundary containing the singularity point O and $q^{(S)}(\mathbf{x}) \equiv \nabla u^{(S)}(\mathbf{x}) \cdot \mathbf{n}(\mathbf{x})$ is its normal derivative. If appropriate functions are chosen for the singular potential solution and its normal derivative then the numerical analysis can be carried out for the regular potential solution $u^{(R)}(\mathbf{x})$ and its normal derivative $q^{(R)}(\mathbf{x}) \equiv \nabla u^{(R)}(\mathbf{x}) \cdot \mathbf{n}(\mathbf{x})$ only. In terms of the regular potential solution $u^{(R)}(\mathbf{x})$, the original inverse problem (1.1)–(1.3) becomes

$$\Delta u^{(R)}(\mathbf{x}) + k^2 u^{(R)}(\mathbf{x}) = 0, \quad \mathbf{x} \in \Omega \tag{15.1}$$

$$u^{(R)}(\mathbf{x}) = \tilde{u}^{\varepsilon}(\mathbf{x}) - u^{(S)}(\mathbf{x}), \quad \mathbf{x} \in \Gamma_D \tag{15.2}$$

$$q^{(R)}(\mathbf{x}) = \tilde{q}^{\varepsilon}(\mathbf{x}) - q^{(S)}(\mathbf{x}), \quad \mathbf{x} \in \Gamma_N. \tag{15.3}$$

The modified boundary conditions (15.2) and (15.3) introduce additional unknowns into the problem, which are the constants of the particular potential solution used to represent the singular solution. It should be noted that these constants are similar to the stress intensity factors corresponding to an analogous problem for the Lamé system and, in what follows, they will be referred to as "flux intensity factors". Since the flux intensity factors are unknown at this stage of the problem, they become primary unknowns.

In order to obtain a unique solution to the regular problem (15.1)–(15.3), it is necessary to specify additional constraints which must be as many as the number of the unknown flux intensity factors, i.e. one for each singular potential solution included in the analysis. These extra conditions must be applied in such a way that the cancelation of the singularity in the regular potential solution is ensured. This is achieved by constraining the regular potential solution and/or its normal derivative directly in a neighbourhood of the singularity point O

$$u^{(R)}(\mathbf{x}) = 0, \quad \mathbf{x} \in \Gamma_N \cap B(O; \tau)$$

$$\text{and/or} \quad q^{(R)}(\mathbf{x}) = 0, \quad \mathbf{x} \in \Gamma_D \cap B(O; \tau), \tag{16}$$

where $B(O; \tau) = \{\mathbf{x} \in \mathbb{R}^2 | \|\mathbf{x}\| < \tau\}$, $\tau > 0$ is sufficiently small and $\| \cdot \|$ represents the Euclidean norm. For example, for the inverse problem (15) the singular potential solution and its normal derivative are expressed, in terms of the polar coordinates (r, θ), as

$$u^{(S)}(\mathbf{x}) \equiv u^{(S)}(r, \theta) = \sum_{n=1}^{n_S} a_n u_n^{(DN)}(r, \theta), \quad q^{(S)}(\mathbf{x}) \equiv q^{(S)}(r, \theta) = \sum_{n=1}^{n_S} a_n\, q_n^{(DN)}(r, \theta), \tag{17}$$

where $u_n^{(DN)}(r, \theta)$ is given by Eq. (12), $q_n^{(DN)}(r, \theta)$ is obtained by taking the normal derivative of $u_n^{(DN)}(r, \theta)$ and a_n, $n = 1, \ldots, n_S$, are the unknown flux intensity factors.

5. Modified method of fundamental solutions

The fundamental solutions $\mathcal{F}_H$ and $\mathcal{F}_{MH}$ of the Helmholtz and modified Helmholtz equations, respectively, in the two-dimensional case are given by, see e.g. Fairweather and Karageorghis [13],

$$\mathcal{F}_H(\mathbf{x}, \mathbf{y}) = \frac{i}{4} H_0^{(1)}(k\|\mathbf{x} - \mathbf{y}\|), \quad \mathbf{x} \in \overline{\Omega}, \ \mathbf{y} \in \mathbb{R}^2 \backslash \overline{\Omega}, \tag{18}$$

and

$$\mathcal{F}_{MH}(\mathbf{x}, \mathbf{y}) = \frac{1}{2\pi} K_0(k\|\mathbf{x} - \mathbf{y}\|), \quad \mathbf{x} \in \overline{\Omega}, \ \mathbf{y} \in \mathbb{R}^2 \backslash \overline{\Omega}, \tag{19}$$

respectively. Here $\mathbf{x} = (x_1, x_2)$ is either a boundary or a domain point, $\mathbf{y} = (y_1, y_2)$ is a source point, $H_0^{(1)}$ is the Hankel function of the first kind of order zero and K_0 is the modified Bessel function of the second kind of order zero.

According to the MFS approach, the regular potential solution, $u^{(R)}$, in the solution domain is approximated by a linear combination of fundamental solutions with respect to M source points $\mathbf{y}^j$ in the form

$$u^{(R)}(\mathbf{x}) \approx \sum_{j=1}^{M} c_j\, \mathcal{F}(\mathbf{x}, \mathbf{y}^j), \quad \mathbf{x} \in \overline{\Omega}, \tag{20}$$

where $\mathcal{F} = \mathcal{F}_H$ in the case of the Helmholtz equation, $\mathcal{F} = \mathcal{F}_{MH}$ in the case of the modified Helmholtz equation, $c_j \in \mathbb{R}$, $j = 1, \ldots, M$, are the unknown coefficients. Then the regular normal flux on the boundary Γ can be approximated by

$$q^{(R)}(\mathbf{x}) \approx \sum_{j=1}^{M} c_j\, \mathcal{G}(\mathbf{x}, \mathbf{y}^j), \quad \mathbf{x} \in \Gamma, \tag{21}$$

where $\mathcal{G}(\mathbf{x}, \mathbf{y}) \equiv \nabla_{\mathbf{x}} \mathcal{F}(\mathbf{x}, \mathbf{y}) \cdot \mathbf{n}(\mathbf{x})$, while $\mathcal{G} = \mathcal{G}_H$ in the case of the Helmholtz equation and $\mathcal{G} = \mathcal{G}_{MH}$ in the case of the modified Helmholtz equation are given by

$$\mathcal{G}_H(\mathbf{x}, \mathbf{y}) =$$
$$-\frac{[(\mathbf{x} - \mathbf{y}) \cdot \mathbf{n}(\mathbf{x})]k\, i}{4\|\mathbf{x} - \mathbf{y}\|} H_1^{(1)}(k\|\mathbf{x} - \mathbf{y}\|), \quad \mathbf{x} \in \Gamma, \quad \mathbf{y} \in \mathbb{R}^2 \backslash \overline{\Omega}, \tag{22}$$

and

$$\mathcal{G}_{MH}(\mathbf{x}, \mathbf{y}) =$$
$$-\frac{[(\mathbf{x} - \mathbf{y}) \cdot \mathbf{n}(\mathbf{x})]k}{2\pi\|\mathbf{x} - \mathbf{y}\|} K_1(k\|\mathbf{x} - \mathbf{y}\|), \quad \mathbf{x} \in \Gamma, \quad \mathbf{y} \in \mathbb{R}^2 \backslash \overline{\Omega}, \tag{23}$$

respectively. Here $H_1^{(1)}$ is the Hankel function of the first kind of order one and K_1 is the modified Bessel function of the second kind of order one.

Assume that the singularity point O is located between the collocation points $\mathbf{x}^{\tilde{n}_D} \in \Gamma_D$ and $\mathbf{x}^{\tilde{n}_N} \in \Gamma_N$, see also Fig. 2, and n_S singular potential solutions $u_n^{(DN)}(r, \theta)$, as well as flux intensities, a_n, are taken into account, such that the additional constraints for the regular potential solution and/or its normal derivative given
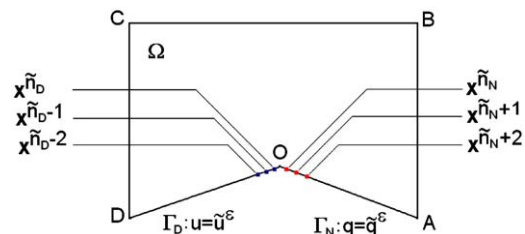

Fig. 2. Schematic diagram of the MFS collocation points in the vicinity of the singularity point O.

by Eq. (16) read as, see e.g. Portela et al. [32], Marin et al. [10] and Marin [30,31],

$$u^{(R)}(\mathbf{x}^{\tilde{n}_N+(1-m)}) = 0, \quad 2m-1 \in \{1,\ldots,n_S\}$$

and $\quad q^{(R)}(\mathbf{x}^{\tilde{n}_D-(1-m)}) = 0, \quad 2m \in \{1,\ldots,n_S\}. \quad (24)$

If n_D collocation points $\mathbf{x}^i$, $i=1,\ldots,n_D$, and n_N collocation points $\mathbf{x}^{n_D+i}$, $i=1,\ldots,n_N$, are chosen on the boundaries Γ_D and Γ_N, respectively, such that $N = n_D + n_N$, and the location of the source points $\mathbf{y}^j$, $j=1,\ldots,M$, is set then the boundary value problem (15.1)–(15.3), together with the additional conditions (16), recasts as a system of $(N+n_S)$ linear algebraic equations with $(M+n_S)$ unknowns which can be generically written as

$$\mathbf{A}\tilde{\mathbf{c}} = \mathbf{F}, \quad (25)$$

where

$$\mathbf{A} = \begin{bmatrix} \mathbf{A}^{(0)} & \mathbf{A}^{(1)} \\ \mathbf{A}^{(2)} & \mathbf{0}_{n_S \times n_S} \end{bmatrix} \in \mathbb{R}^{(N+n_S)\times(M+n_S)}, \quad \tilde{\mathbf{c}} = \begin{pmatrix} \mathbf{c}^{(0)} \\ \mathbf{a} \end{pmatrix} \in \mathbb{R}^{M+n_S}, \quad \mathbf{F} = \begin{pmatrix} \mathbf{F}^{(0)} \\ \mathbf{0}_{n_S} \end{pmatrix} \in \mathbb{R}^{N+n_S}, \quad (26)$$

with the unknown vectors $\mathbf{c}^{(0)} = (c_1,\ldots,c_M)^T \in \mathbb{R}^M$ and $\mathbf{a} = (a_1,\ldots,a_{n_S})^T \in \mathbb{R}^{n_S}$. The components of the matrices $\mathbf{A}^{(0)} \in \mathbb{R}^{N\times M}$, $\mathbf{A}^{(1)} \in \mathbb{R}^{N\times n_S}$, and $\mathbf{A}^{(2)} \in \mathbb{R}^{n_S\times M}$, and the vector $\mathbf{F}^{(0)} \in \mathbb{R}^N$ in Eq. (26) are given by

$$A_{ij}^{(0)} = \begin{cases} \mathcal{F}(\mathbf{x}^i,\mathbf{y}^j), & i=1,\ldots,n_D, & j=1,\ldots,M \\ \mathcal{G}(\mathbf{x}^i,\mathbf{y}^j), & i=n_D+1,\ldots,n_D+n_N, & j=1,\ldots,M \end{cases} \quad (27.1)$$

$$A_{ij}^{(1)} = \begin{cases} u_j^{(DN)}(r^i,\theta^i), & i=1,\ldots,n_D, & j=1,\ldots,M \\ q_j^{(DN)}(r^i,\theta^i), & i=n_D+1,\ldots,n_D+n_N, & j=1,\ldots,M \end{cases} \quad (27.2)$$

$$A_{ij}^{(2)} = \begin{cases} \mathcal{F}(\mathbf{x}^{\tilde{n}_N+(1-m)},\mathbf{y}^j), & i=2m-1 \in \{1,\ldots,n_S\}, & j=1,\ldots,M \\ \mathcal{G}(\mathbf{x}^{\tilde{n}_D-(1-m)},\mathbf{y}^j), & i=2m \in \{1,\ldots,n_S\}, & j=1,\ldots,M \end{cases} \quad (27.3)$$

$$F_i^{(0)} = \begin{cases} \tilde{u}^\varepsilon(\mathbf{x}^i), & i=1,\ldots,n_D \\ \tilde{q}^\varepsilon(\mathbf{x}^i), & i=n_D+1,\ldots,n_D+n_N \end{cases} \quad (27.4)$$

where (r^i,θ^i) are the local polar coordinates of the collocation point $\mathbf{x}^i$, $i=1,\ldots,N$. Note that the matrix $\mathbf{A}^{(0)}$, and the vectors $\mathbf{c}^{(0)}$ and $\mathbf{F}^{(0)}$ in (26) correspond to the standard MFS, i.e. $n_S = 0$, applied to solving the regular inverse problem (15.1)–(15.3).

In order to uniquely determine the solution $\tilde{\mathbf{c}}$ of the system of linear algebraic Eq. (25), i.e. the coefficients c_j, $j=1,\ldots,M$, in approximations (20) and (21) and the flux intensity factors a_n, $n=1,\ldots,n_S$, in the asymptotic expansions (17), the total number of collocation points corresponding to the Dirichlet and Neumann boundary conditions, N, and the number of source points, M, must satisfy the inequality $M \leq N$.

To implement the MFS, the location of the source points has to be determined and this is usually achieved by considering either the static or the dynamic approach. In the static approach, the source points are pre-assigned and kept fixed throughout the solution process, this approach reducing to solving a linear problem [13]. In the dynamic approach, the source points and the unknown coefficients are determined simultaneously during the solution process via a system of nonlinear equations which may be solved using minimization methods [13]. Recently, Gorzelańczyk and Kołodziej [34] thoroughly investigated the performance of the MFS with respect to the shape of the pseudo-boundary on which the source points are situated, proving that, for the same number of boundary collocation points and sources, more accurate results are obtained if the shape of the pseudo-boundary is similar to that of the boundary of the solution domain. Therefore, we have decided to employ the static approach in our computations, at the same time accounting for the findings of Gorzelańczyk and Kołodziej [34].

6. Regularization

As a direct consequence of the fact that the singular inverse problem (1.1)–(1.3), as well as its regular version (15.1)–(15.3), is highly ill-posed, the MFS discretization matrix $\mathbf{A}$ is severely ill-conditioned. Hence a direct approach to solving the resulting MFS system of linear algebraic equations (25), such as the LSM, would produce highly oscillatory and unbounded solutions, i.e. unstable solutions. The LSM solution to the MFS system (25) is sought as, see e.g. Tikhonov and Arsenin [35]

$$\tilde{\mathbf{c}}_{LSM}: \quad \mathcal{T}_{LSM}(\tilde{\mathbf{c}}_{LSM}) = \min_{\tilde{\mathbf{c}} \in \mathbb{R}^{M+n_S}} \mathcal{T}_{LSM}(\tilde{\mathbf{c}}), \quad (28)$$

where $\mathcal{T}_{LSM}$ is the LSM functional given by

$$\mathcal{T}_{LSM}: \mathbb{R}^{M+n_S} \longrightarrow [0,\infty), \quad \mathcal{T}_{LSM}(\tilde{\mathbf{c}}) = \|\mathbf{A}\tilde{\mathbf{c}} - \mathbf{F}\|^2. \quad (29)$$

Formally, the LSM solution, $\tilde{\mathbf{c}}_{LSM}$, of the minimization problem (28) is given as the solution of the following system of linear algebraic equations:

$$(\mathbf{A}^T\mathbf{A})\tilde{\mathbf{c}} = \mathbf{A}^T\mathbf{F}, \quad (30)$$

in the sense that

$$\tilde{\mathbf{c}}_{LSM} = (\mathbf{A}^T\mathbf{A})^{-1}\mathbf{A}^T\mathbf{F}. \quad (31)$$

The accurate and stable solution of the system of linear algebraic equations (25) is very important for obtaining physically meaningful numerical results. Regularization methods are among the most popular and successful methods for solving stably and accurately ill-conditioned matrix equations [35]. In the present computations, we use the TRM to solve the matrix equation arising from the MFS discretization. The Tikhonov regularized solution to the system of linear algebraic equations (25) is sought as [35]

$$\tilde{\mathbf{c}}_\lambda: \mathcal{T}_\lambda(\tilde{\mathbf{c}}_\lambda) = \min_{\tilde{\mathbf{c}} \in \mathbb{R}^{M+n_S}} \mathcal{T}_\lambda(\tilde{\mathbf{c}}), \quad (32)$$

where $\mathcal{T}_\lambda$ is the zeroth-order Tikhonov functional given by

$$\mathcal{T}_\lambda(\cdot): \mathbb{R}^{M+n_S} \longrightarrow [0,\infty),$$
$$\mathcal{T}_\lambda(\tilde{\mathbf{c}}) = \mathcal{T}_{LSM}(\tilde{\mathbf{c}}) + \lambda^2\|\tilde{\mathbf{c}}\|^2 = \|\mathbf{A}\tilde{\mathbf{c}} - \mathbf{F}\|^2 + \lambda^2\|\tilde{\mathbf{c}}\|^2, \quad (33)$$

and $\lambda > 0$ is the regularization parameter to be chosen. Formally, for a given value of the regularization parameter, λ, the Tikhonov regularized solution $\tilde{\mathbf{c}}_\lambda$ of the problem (32) is obtained by solving the normal equation

$$(\mathbf{A}^T\mathbf{A} + \lambda^2\mathbf{I}_{M+n_S})\tilde{\mathbf{c}} = \mathbf{A}^T\mathbf{F}, \quad (34)$$

namely

$$\tilde{\mathbf{c}}_\lambda = (\mathbf{A}^T\mathbf{A} + \lambda^2\mathbf{I}_{M+n_S})^{-1}\mathbf{A}^T\mathbf{F}, \quad (35)$$

where $\mathbf{I}_{M+n_S}$ is the identity matrix. Note that the LSM solution is a limit case of the TRM solution as $\lambda \longrightarrow 0$.

The performance of regularization methods depends crucially on the suitable choice of the regularization parameter. One extensively studied criterion is Morozov's discrepancy principle [36]. Although this criterion is mathematically rigorous, it requires a reliable estimation of the amount of noise added into the data which may not be available in practical problems. Heuristical approaches are preferable in the case when no *a priori* information about the noise is available. For the TRM, several heuristical approaches have been proposed, including the generalized cross-validation [37] and Hansen's L-curve criterion [38]. In this paper, we employ the L-curve criterion to determine the optimal regularization parameter, λ_{opt}. If we define on a

logarithmic scale the curve $\{(\|\mathbf{A}\tilde{\mathbf{c}}_\lambda - \mathbf{F}\|, \|\tilde{\mathbf{c}}_\lambda\|)|\lambda > 0\}$ then this typically has an L-shaped form and hence it is referred to as the L-curve. According to the L-curve criterion, the optimal regularization parameter corresponds to the corner of the L-curve since a good tradeoff between the residual and solution norms is achieved at this point. Herein, we employ the algorithm of Hansen [38], which is based on fitting a parametric cubic spline to the discrete points and then taking the point corresponding to the maximum curvature of the L-curve to be its corner.

7. Numerical results and discussion

It is the purpose of this section to present the performance of the modified MFS described in Section 5. To do so, we solve numerically the inverse boundary value problem (1.1)–(1.3) associated with two-dimensional Helmholtz-type equations in the presence of boundary singularities.

7.1. Examples

In the case of the singular inverse problems for both the Helmholtz and the modified Helmholtz equations analysed herein, the solution domains under consideration, Ω, accessible boundaries, Γ_D and Γ_N, and corresponding analytical solutions for $u^{(an)}(\mathbf{x})$ are given as follows:

Example 1. N–D singularity for the modified Helmholtz equation ($k = 1$) in the rectangle $\Omega = ABCD = (-1, 1) \times (0, 1)$ containing an edge crack OA, see Fig. 1(a):

$$u^{(an)}(\mathbf{x}) = u_1^{(ND)}(\mathbf{x}) - 1.30 u_2^{(ND)}(\mathbf{x}) + 1.50 u_3^{(ND)}(\mathbf{x})$$
$$- 1.70 u_4^{(ND)}(\mathbf{x}), \quad \mathbf{x} \in \overline{\Omega}. \tag{36}$$

Example 2. D–D singularity for the modified Helmholtz equation ($k = 1$) in the L-shaped domain $\Omega = OABCDE = (-1, 1) \times (0, 1) \cup (-1, 0) \times (-1, 0]$, see Fig. 1(b):

$$u^{(an)}(\mathbf{x}) = u_1^{(DD)}(\mathbf{x}) - 1.30 u_2^{(DD)}(\mathbf{x}) - 1.70 u_4^{(DD)}(\mathbf{x}), \quad \mathbf{x} \in \overline{\Omega}. \tag{37}$$

Example 3. D–N singularity for the Helmholtz equation ($k = 1$) in the rectangle containing a V-notch with the re-entrant angle $\pi/6$ $\Omega = OABCD = (-1, 1) \times (0, 1) \backslash \Delta ODD'$, see Fig. 1(c):

$$u^{(an)}(\mathbf{x}) = u_2^{(DN)}(\mathbf{x}) - 1.50 u_3^{(DN)}(\mathbf{x}) + 1.30 u_4^{(DN)}(\mathbf{x}), \quad \mathbf{x} \in \overline{\Omega}. \tag{38}$$

It should be mentioned that the functions $u_i^{(ND)}$, $u_i^{(DD)}$ and $u_i^{(DN)}$, $i = 1, \ldots, 4$, used in expressions (36)–(38) are defined in Eqs. (10)–(12), respectively. It is important to notice that all examples analysed in this study contain a singularity at the origin O. Moreover, this singularity is caused by the nature of the analytical solutions considered, i.e. the analytical solutions are given as linear combinations of the first four singular solutions satisfying homogeneous boundary conditions on the edges of the wedge, as well as by a sharp corner in the boundary (Examples 2 and 3) or by an abrupt change in the boundary conditions at O (Examples 1 and 3), see Figs. 1(a)–(c). For all examples considered, it can be seen that the boundary $\Gamma_C = \Gamma_D \cap \Gamma_N$ is over-specified by prescribing on it both the boundary solution, $u|_{\Gamma_C}$, and the normal flux, $q|_{\Gamma_C}$, whilst the boundary BC is under-specified since neither the boundary solution, $u|_{BC}$, nor the normal flux, $q|_{BC}$, is known and has to be determined.

The singular inverse problems investigated in this paper have been solved using a uniform distribution of both the boundary collocation points $\mathbf{x}^i$, $i = 1, \ldots, N$, and the source points $\mathbf{y}^j$, $j = 1, \ldots, M$, with the mention that the latter were located on a so-called pseudo-boundary, Γ_S, which has the same shape as the

boundary Γ of the solution domain and is situated at the distance $d = 3$ from Γ, see also Gorzelańczyk and Kołodziej [34]. Furthermore, the number of boundary collocation points was set to:

(i) $N = 120$ for Examples 1 and 3, such that $N/3 = 40$ and $N/6 = 20$ collocation points are situated on each of the boundaries BC and OA, AB, CD and DO, respectively;

(ii) $N = 154$ for Example 2, such that 19 and 39 collocation points are situated on each of the boundaries OA, AB, DE and EO, and BC and CD, respectively.

In addition, for all examples investigated throughout this study, the number of source points, M, was taken to be equal to that of the boundary collocation points, N, i.e. $M = N$.

7.2. Accuracy errors

In what follows, we denote by $u^{(num)}$ and $q^{(num)}$ the numerical values for the potential solution and normal flux, respectively, obtained using the LSM, i.e. by a direct inversion method, and by subtracting the first $n_S \geq 0$ singular potential solutions, with the convention that when $n_S = 0$ then the numerical potential solution and normal flux are obtained using the standard MFS, i.e. without removing the singularity.

In order to measure the accuracy of the numerical approximation for the potential solution, $u^{(num)}$, and normal flux, $q^{(num)}$, with respect to their corresponding analytical values, $u^{(an)}$, and, $q^{(an)}$, respectively, we define the *relative root mean-square (RMS) errors* by

$$e_u(\Gamma_j) = \sqrt{\sum_{j=1}^{N_j} (u^{(num)}(\mathbf{x}^j) - u^{(an)}(\mathbf{x}^j))^2 \bigg/ \sum_{j=1}^{N_j} (u^{(an)}(\mathbf{x}^j))^2} \tag{39}$$

$$e_q(\Gamma_j) = \sqrt{\sum_{j=1}^{N_j} (q^{(num)}(\mathbf{x}^j) - q^{(an)}(\mathbf{x}^j))^2 \bigg/ \sum_{j=1}^{N_j} (q^{(an)}(\mathbf{x}^j))^2} \tag{40}$$

where N_j is the number of collocation points on the boundary $\Gamma_j \subset \Gamma$.

Furthermore, we also define the *normalized errors*

$$\mathrm{err}(u(\mathbf{x})) = \frac{|u^{(num)}(\mathbf{x}) - u^{(an)}(\mathbf{x})|}{\max_{\mathbf{y} \in \tilde{\Gamma}} |u^{(an)}(\mathbf{y})|}, \quad \mathrm{err}(q(\mathbf{x})) = \frac{|q^{(num)}(\mathbf{x}) - q^{(an)}(\mathbf{x})|}{\max_{\mathbf{y} \in \tilde{\Gamma}} |q^{(an)}(\mathbf{y})|}, \tag{41}$$

for the potential solution and normal flux, respectively, where $\tilde{\Gamma}$ denotes the set of boundary collocation points, since on using these errors divisions by zero and very high errors at points where the potential solution and/or normal flux have relatively small values are avoided.

In addition, we introduce an error that measures the inaccuracies in the numerical results obtained for the flux intensity factors, namely the *absolute error* defined by

$$\mathrm{Err}(a_j) = |a_j^{(num)} - a_j|. \tag{42}$$

Here $a_j^{(num)}$ represents the numerical value for the exact flux intensity factor a_j, provided that the latter is available.

7.3. Effect of the singularity subtraction technique

The first example investigated contains a singularity at the boundary point O caused by both the abrupt change in the boundary conditions and the nature of the analytical solution, see Eq. (36), in the case of the modified Helmholtz equation. It should be noted that this singularity is of a form which is similar to the case of a sharp re-entrant corner of angle zero. This may be seen

by extending the domain $\Omega = (-1, 1) \times (0, 1)$ using symmetry with respect to the x_1- axis, see also Fig. 1(a). In this way, a problem is obtained for a square domain containing a crack, namely $\tilde{\Omega} = (-1, 1) \times (-1, 1) \backslash [0, 1] \times \{0\}$ with zero flux boundary conditions along the crack $[0, 1] \times \{0\}$. This problem may also be treated by considering the domain $\tilde{\Omega}$ described above, with the mention that the singular functions (9) corresponding to Neumann–Neumann boundary conditions along the crack must be used.

However, the original domain Ω and the mixed boundary conditions illustrated in Fig. 1(a) have been considered in our analysis, i.e. $\theta_1 = 0$ and $\theta_2 = \pi$.

If the LSM is applied to solving the singular inverse problem given by Example 1 subject to noisy data without subtracting any singular potential solutions ($n_S = 0$) then the numerical solution retrieved by this direct solution method is not only inaccurate, but also unstable. This aspect, which is strongly related to the
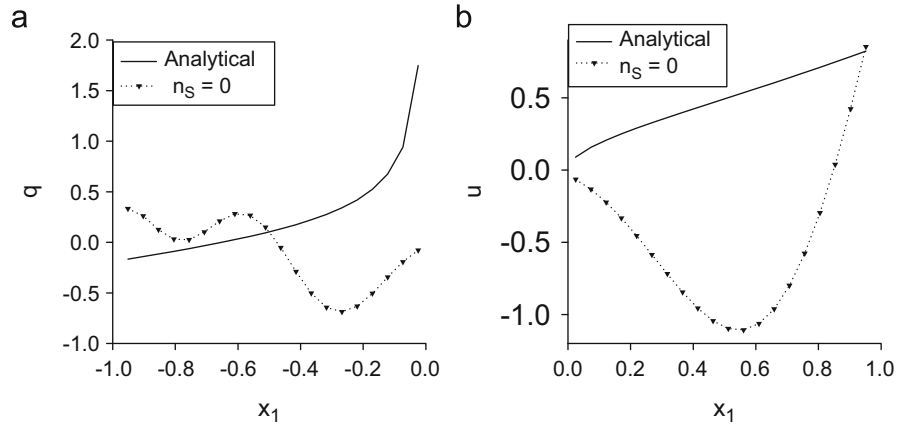

Fig. 3. Analytical and numerical solutions for (a) $q|_{DO}$ and (b) $u|_{OA}$, obtained using the LSM, $n_S = 0$ and $p_q = 1\%$ noise added into the Neumann data $q|_{\Gamma_N}$, for Example 1.
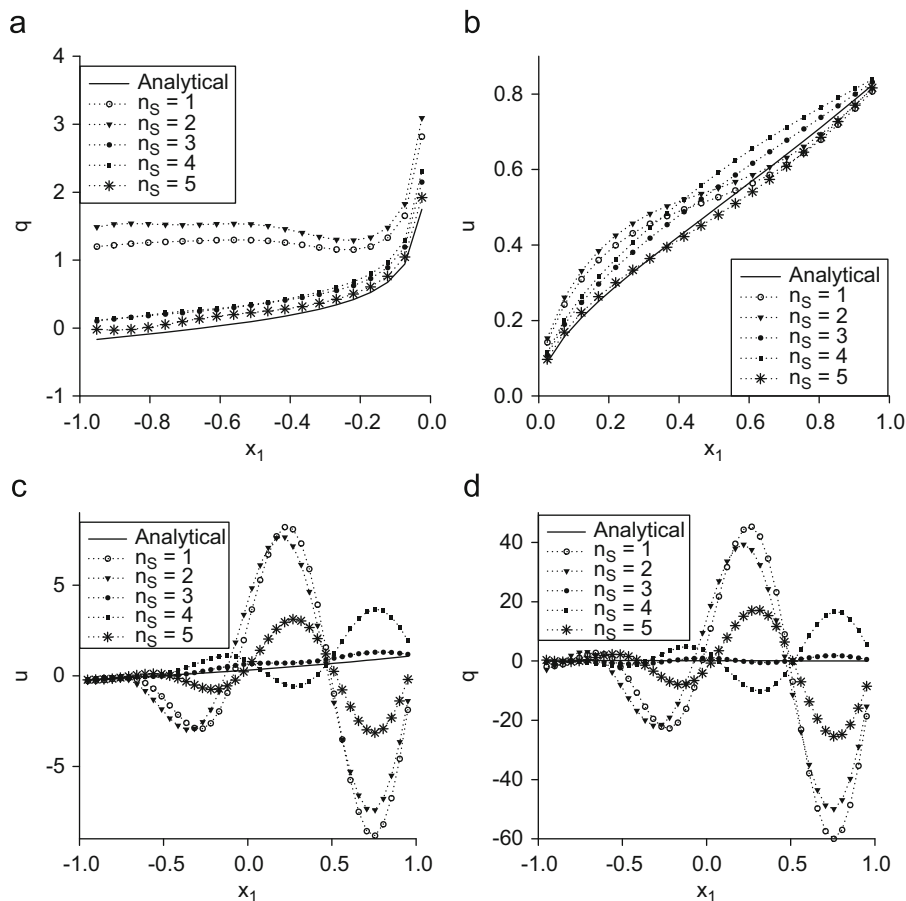

Fig. 4. Analytical and numerical solutions for (a) $q|_{DO}$, (b) $u|_{OA}$, (c) $u|_{BC}$, and (d) $q|_{BC}$, obtained using the LSM, $n_S \in \{1, 2, 3, 4, 5\}$ and $p_q = 1\%$ noise added into the Neumann data $q|_{\Gamma_N}$, for Example 1.
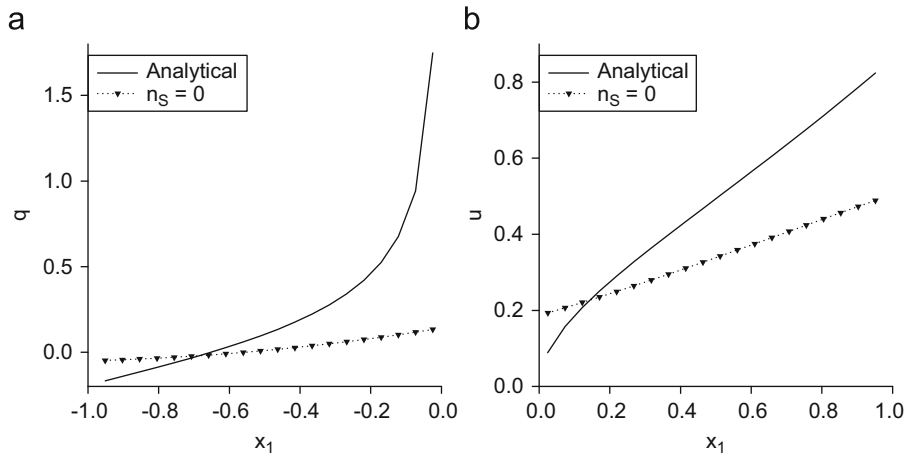
Fig. 5. Analytical and numerical solutions for (a) $q|_{DO}$ and (b) $u|_{OA}$, obtained using the TRM, $n_S = 0$ and $p_q = 1\%$ noise added into the Neumann data $q|_{\Gamma_N}$, for Example 1.
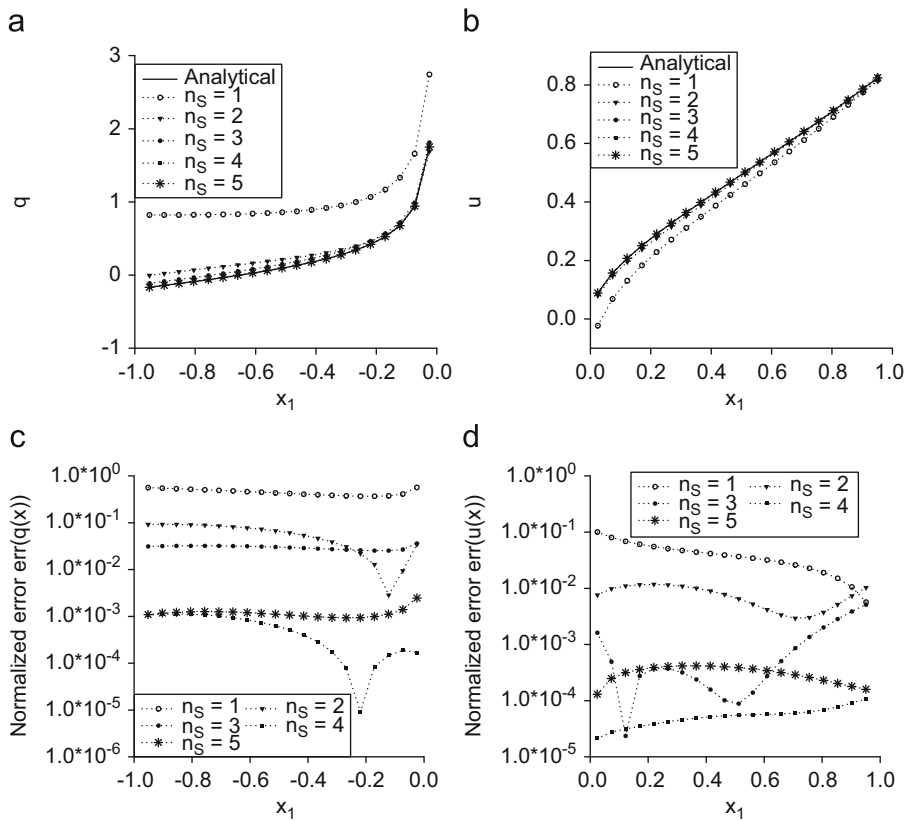

Fig. 6. Analytical and numerical solutions for (a) $q|_{DO}$ and (b) $u|_{OA}$, and the corresponding normalized errors (c) err$(q(\mathbf{x}))$, $\mathbf{x} \in$ DO, and (d) err$(u(\mathbf{x}))$, $\mathbf{x} \in$ OA, obtained using the TRM, $n_S \in \{1, 2, 3, 4, 5\}$ and $p_q = 1\%$ noise added into the Neumann data $q|_{\Gamma_N}$, for Example 1.

ill-posedness of the inverse problem [33] and hence the impossibility of the standard MFS system to represent corner singularities, can be clearly noticed from Figs. 3(a) and (b) that present the analytical and LSM-based numerical normal flux and potential solution on the wedges DO and OA, respectively, when the Neumann data $q|_{\Gamma_N} = q|_{AB \cup CD}$ was perturbed by $p_q = 1\%$ noise.

Figs. 4(a) and (b) illustrate a comparison between the analytical and numerical solutions for $q|_{DO}$ and $u|_{OA}$, respectively, obtained with $p_q = 1\%$ and by removing various numbers of singular potential solutions, namely $n_S \in \{1, 2, 3, 4, 5\}$, for the N–D singular inverse problem given by Example 1. It can be seen from these figures that the numerical results for both $q|_{DO}$

and $u|_{OA}$ are considerably improved, even if only the first singular potential solution corresponding to Dirichlet–Neumann boundary conditions on $(-1, 1) \times \{0\}$ is removed, i.e. $n_S = 1$. The same pattern is observed if one continues to remove higher-order singular potential solutions in the modified MFS, i.e. $n_S \in \{2, 3\}$, as can be seen from Figs. 4(a) and (b). Moreover, the removal of $n_S \geq 4$ singular potential solutions from the standard MFS ensures the retrieval of reasonably accurate numerical solutions for the normal flux on DO and the potential solution on OA, respectively, see Figs. 4(a) and (b). However, very inaccurate and highly oscillatory solutions have been obtained for both the unknown potential solution and normal flux on the under-specified

boundary BC and these are presented in Figs. 4(c) and (d), respectively.

Although not presented, it is reported that similar results have been obtained for the other examples investigated in this study. Therefore, in order to retrieve accurate and stable numerical solutions for singular inverse problem associated with Helmholtz-type equations, the use of the SST in the modified MFS approach only is not sufficient, as clearly shown in Figs. 4(a)–(d).

7.4. Effect of the Tikhonov regularization

If solely the TRM is employed to solve the resulting MFS system (25) without removing any singular potential solutions then again very inaccurate numerical results have been retrieved for both the potential solution and the normal flux. These results are presented in Figs. 5(a) and (b) which illustrate the analytical and numerical normal flux and potential solution on the wedges DO and OA, respectively, when $q|_{\Gamma_N} = q|_{AB \cup CD}$ was perturbed by $p_q = 1\%$ noise and $n_S = 0$, in the case of Example 1. By comparing Figs. 3–5, we can conclude that both the SST and the TRM should be employed in order to solve the singular inverse problem given by Example 1 in a stable and accurate manner.

Indeed, if these two techniques are used together then the difficulties caused by the ill-posedness of the inverse problem, as well as the boundary singularity at O, can be overcome. Figs. 6(a) and (b) present the analytical and numerical results for the normal flux on DO and potential solution on OA, respectively, retrieved by solving the MFS + SST system of linear algebraic equations (25) using the TRM, in conjunction with the L-curve criterion for choosing the optimal regularization parameter, $p_q = 1\%$ and $n_S \in \{1, 2, 3, 4, 5\}$, in the case of Example 1. From these figures it can be noticed that the effect of SST in the presence of the TRM is remarkable. When the TRM is employed then even the removal of the first two singular potential solutions, i.e. $n_S = 2$, provides a very accurate numerical approximation for the potential solution $u|_{OA}$, which is also bounded and exempted from oscillations. Similar estimations are also valid for the numerical normal flux $q|_{DO}$, with the mention that, as expected, the numerical results obtained for the normal flux on DO are more inaccurate than those retrieved for the potential solution on OA. The same conclusion can also be drawn from Figs. 6(c) and (d) which present the results shown in Figs. 6(a) and (b) in terms of the normalized errors $err(q(\mathbf{x}))$, $\mathbf{x} \in DO$, and $err(u(\mathbf{x}))$, $\mathbf{x} \in OA$, respectively, as defined by formula (41). On comparing Figs. 3–6, we can conclude that the TRM provides very accurate MFS + SST-based numerical solutions to singular inverse problems for Helmholtz-type equations, at the same time having a regularizing/stabilizing effect on the MFS + SST solutions to such problems.

7.5. Choice of the optimal regularization parameter

Figs. 7(a) and (b) illustrate the relative RMS errors $e_u(BC)$ and $e_q(BC)$, respectively, given by relations (39) and (40), as functions
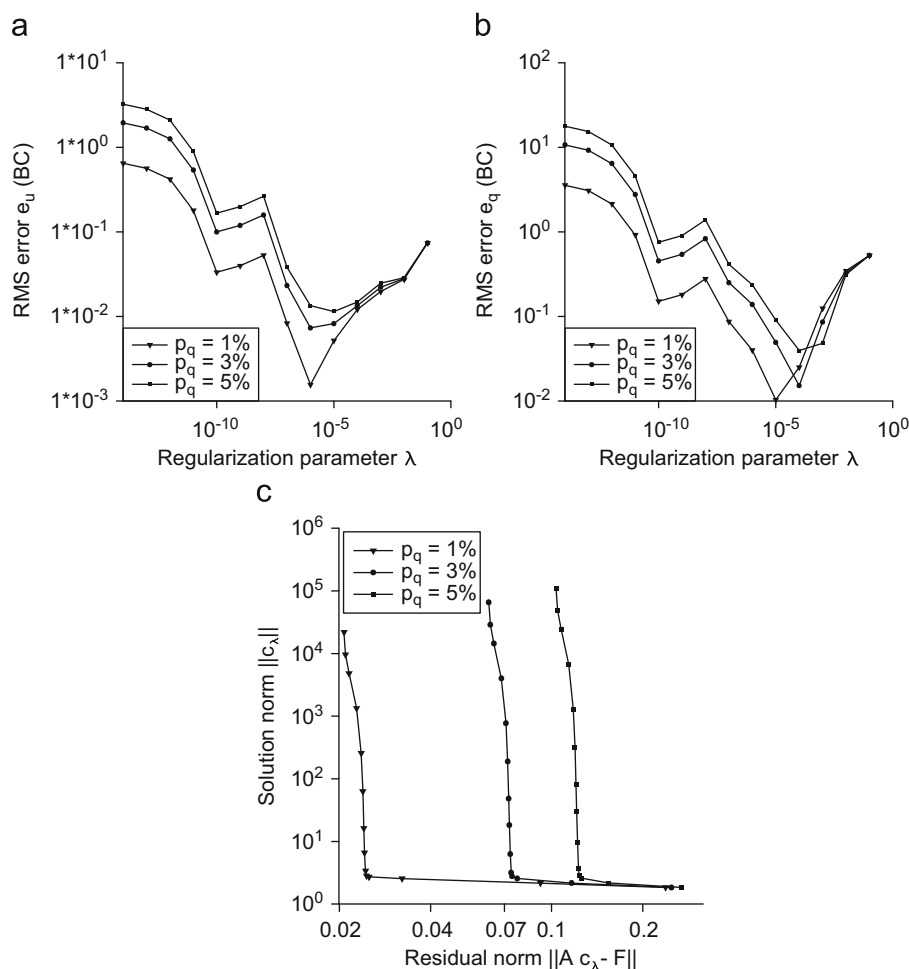

Fig. 7. The RMS errors: (a) $e_u(BC)$, (b) $e_q(BC)$, and (c) the corresponding L-curve, obtained using the TRM, $n_S = 5$ and various levels of noise added into the Neumann data, $q|_{\Gamma_N}$, namely $p_q \in \{1\%, 3\%, 5\%\}$, for Example 1.

of the regularization parameter λ, obtained with $n_S = 5$ and various levels of noise added into the input normal flux data $q|_{\Gamma_N}$, for the inverse problem given by Example 1. From these figures it can be seen that both errors $e_u(BC)$ and $e_q(BC)$ decrease as the level of noise p_q added into the input Neumann data decreases for all regularization parameters λ and $e_u(BC) < e_q(BC)$ for all regularization parameters λ and a fixed amount p_q of noise added into the input normal flux data $q|_{\Gamma_N}$, i.e. the numerical results obtained for the normal flux are more inaccurate than those retrieved for the potential solution on the under-specified boundary BC. Fig. 7(c) shows on a log–log scale the L-curves obtained for $n_S = 5$ and various levels of noise added into the input normal flux data in the case of Example 1. By comparing this

figure with Figs. 7(a) and (b), it can be seen, for various levels of noise, that the "corner" of the L-curve occurs at about the same value of the regularization parameter λ where the minimum in the accuracy errors $e_u(BC)$ and $e_q(BC)$ is attained. Hence the choice of the optimal regularization parameter λ_{opt} according to the L-curve criterion is fully justified. Similar results have been obtained for the Cauchy problems given by Examples 2 and 3 and therefore they are not presented here.

Table 1 presents the values of the relative RMS errors $e_u(BC)$ and $e_q(BC)$ obtained by both methods, namely the LSM and the TRM, with $n_S = 5$ and various levels of noise added into the input normal flux data $q|_{\Gamma_N}$, namely $p_q \in \{1\%, 3\%, 5\%\}$, in the case of Example 1, as well as the optimal values for the regularization parameter λ. By considering this table and Figs. 3–6, we can conclude that the use of regularization methods, in conjunction with the SST+MFS approach, is fully justified and provides both stable and accurate numerical results not only on the edges sharing the singularity point, but also on the under-specified boundary BC.

7.6. Numerical stability of the method

In order to investigate the numerical stability of the proposed modified MFS algorithm described in Section 5, in conjunction with the L-curve method of Hansen [38] for selecting the optimal value for the regularization parameter, λ, in what follows we consider the inverse problems given by Examples 1–3, the
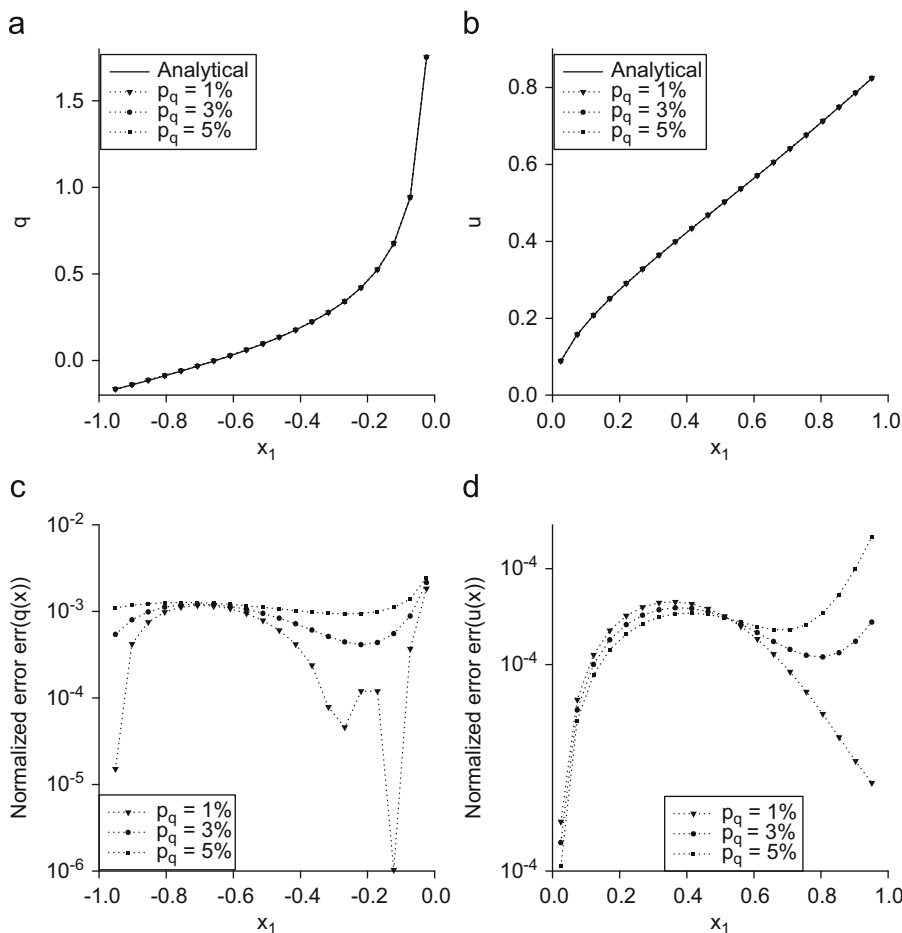
Table 1
The relative RMS errors, $e_u(BC)$ and $e_q(BC)$, and the values for the corresponding optimal regularization parameter, λ_{opt}, obtained using the LSM and TRM, $n_S = 5$ and various levels of noise added into the normal flux $q|_{\Gamma_N}$, namely $p_q \in \{1\%, 3\%, 5\%\}$, for Example 1.

Method	p_q (%)	e_u (BC)	e_q (BC)	λ_{opt}
LSM	1	0.33621×10^1	0.78192×10^2	–
	3	0.10086×10^2	0.23457×10^3	–
	5	0.16809×10^2	0.39093×10^3	–
TRM	1	0.51874×10^{-2}	0.10351×10^{-1}	1.0×10^{-5}
	3	0.82568×10^{-2}	0.49427×10^{-1}	1.0×10^{-5}
	5	0.11467×10^{-1}	0.90614×10^{-1}	1.0×10^{-5}

Fig. 8. Analytical and numerical solutions for (a) $q|_{DO}$ and (b) $u|_{OA}$, and the corresponding normalized errors (c) err($q(\mathbf{x})$), $\mathbf{x} \in DO$, and (d) err($u(\mathbf{x})$), $\mathbf{x} \in OA$, obtained using the TRM, $n_S = 5$ and various levels of noise added into the Neumann data, $q|_{\Gamma_N}$, namely $p_q \in \{1\%, 3\%, 5\%\}$, for Example 1.

Fig. 9. Analytical and numerical solutions for (a) $u|_{BC}$ and (b) $q|_{BC}$, and the corresponding normalized errors (c) err($u(\mathbf{x})$), $\mathbf{x} \in$ BC, and (d) err($q(\mathbf{x})$), $\mathbf{x} \in$ BC, obtained using the TRM, $n_S = 5$ and various levels of noise added into the Neumann data, $q|_{\Gamma_N}$, namely $p_q \in \{1\%, 3\%, 5\%\}$, for Example 1.
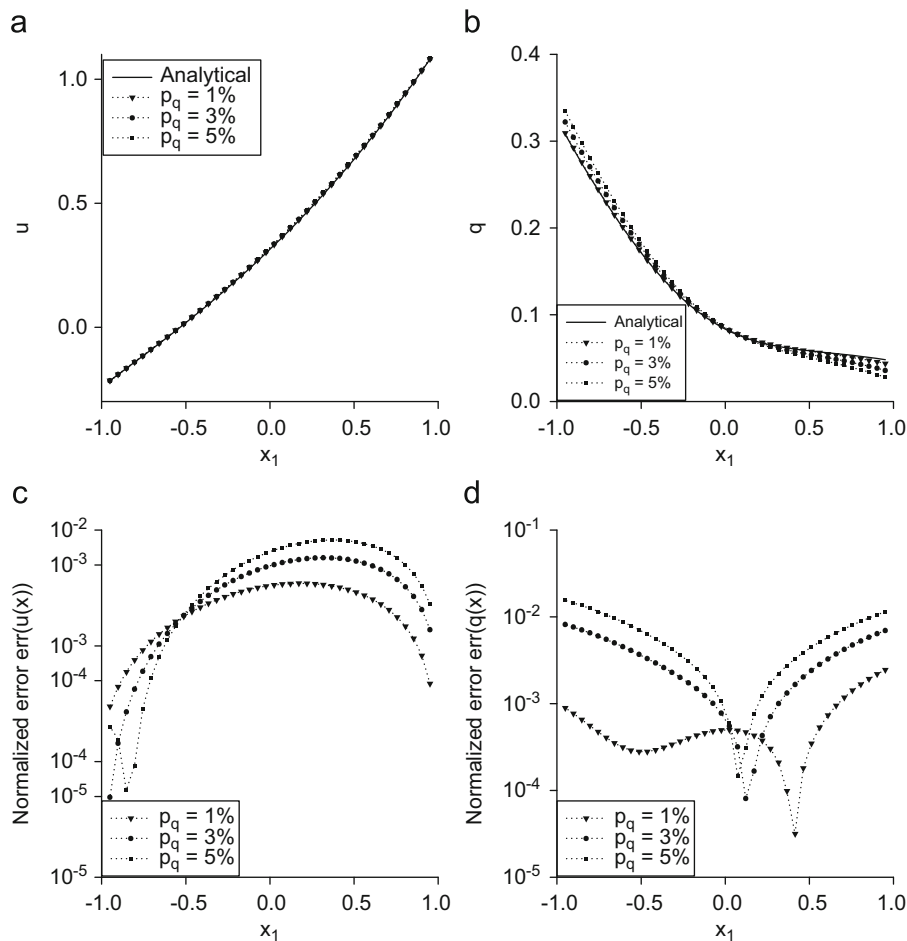
Table 2

The numerically retrieved values, $a_j^{(num)}$, for the flux intensity factors and the corresponding absolute errors, Err(a_j), obtained using the TRM , $n_S = 5$ and various levels of noise added into the normal flux $q|_{\Gamma_N}$, namely $p_q \in \{1\%, 3\%, 5\%\}$, for Example 1.

p_q (%)	$a_1^{(num)}$	Err(a_1)	$a_2^{(num)}$	Err(a_2)	$a_3^{(num)}$	Err(a_3)	$a_4^{(num)}$	Err(a_4)
1	1.0027	0.27×10^{-2}	-1.3009	0.85×10^{-3}	1.5182	0.18×10^{-1}	-1.6997	0.29×10^{-3}
3	1.0031	0.31×10^{-2}	-1.2988	0.12×10^{-2}	1.5472	0.47×10^{-1}	-1.7833	0.83×10^{-1}
5	1.0036	0.36×10^{-2}	-1.2967	0.37×10^{-2}	1.5761	0.76×10^{-1}	-1.8670	0.17×10^{0}

corresponding MFS discretizations mentioned in Section 7.1 and $n_S = 5$, whilst at the same time varying the level of noise added into the Dirichlet or Neumann data as $p_u, p_q \in \{1\%, 3\%, 5\%\}$.

Figs. 8(a) and (b) present the numerical normal flux on the boundary DO and potential solution on the boundary OA, respectively, obtained using the MFS+SST algorithm for various levels of Gaussian random noise added into the normal flux $q|_{\Gamma_N}$, in the case of Example 1, in comparison with their analytical values. From these figures it can be seen that, for all amounts, p_q, of noise added into $q|_{\Gamma_N}$, both the numerical potential solution on OA and the normal flux on DO represent excellent approximations for their analytical counterparts, being at the same time exempted from high and unbounded oscillations in the vicinity of the singularity. Similar conclusions can be drawn from Figs. 8(c) and (d) which show the normalized errors err($q(\mathbf{x})$), $\mathbf{x} \in$ DO, and

err($u(\mathbf{x})$), $\mathbf{x} \in$ OA, respectively, associated with the numerical results illustrated in Figs. 8(a) and (b). The numerical potential solution and normal flux on the under-specified boundary BC, as well as their corresponding normalized errors, obtained using the regularized MFS+SST and $p_q \in \{1\%, 3\%, 5\%\}$, are illustrated in Figs. 9(a)–(d). From these figures we can conclude that the numerical results for the potential solution and normal flux on the under-specified boundary BC are also in very good agreement with their corresponding exact values and, in addition, they are convergent and stable with respect to decreasing the amount of noise added into the input boundary normal flux $q|_{\Gamma_N}$. Accurate, stable and convergent numerical results with respect to decreasing p_q have also been obtained for the flux intensity factors $a_j, j = 1, \ldots, 4$, and these, together with their associated absolute errors Err(a_j), $j = 1, \ldots, 4$, are presented in Table 2.
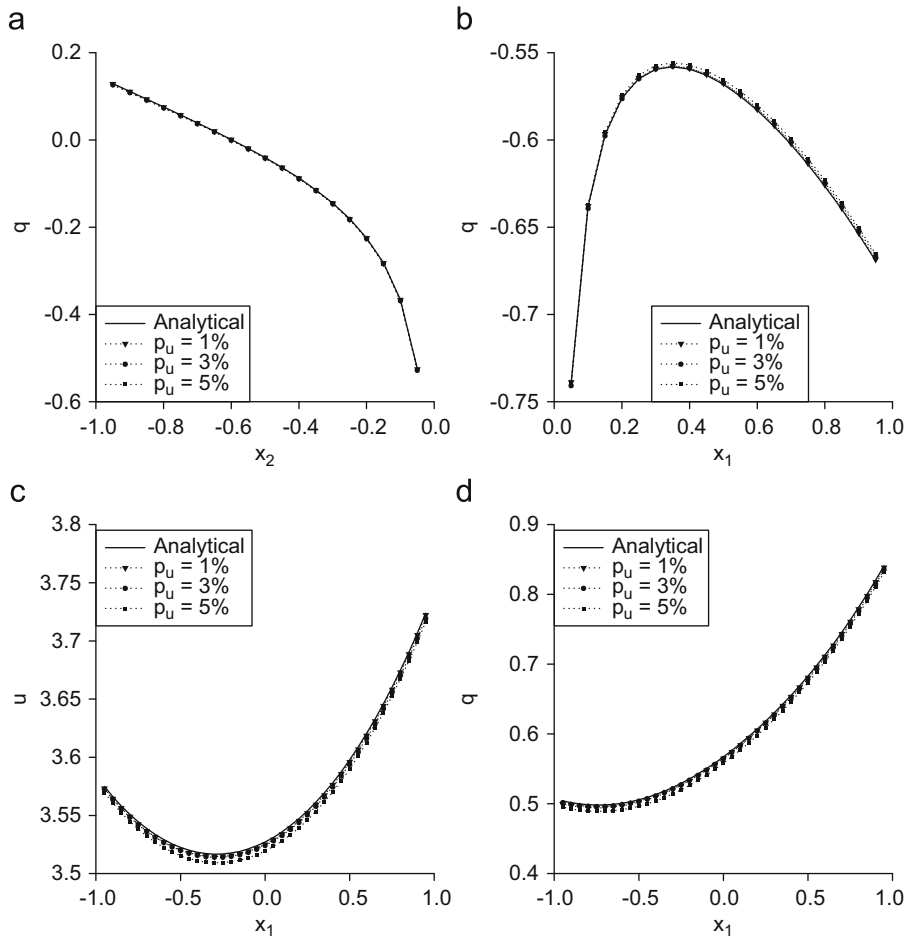
Fig. 10. Analytical and numerical solutions for (a) $q|_{EO}$, (b) $q|_{OA}$, (c) $u|BC$, and (d) $q|BC$, obtained using the TRM, $n_S = 5$ and various levels of noise added into the Dirichlet data, $u|_{\Gamma_D}$, namely $p_u \in \{1\%, 3\%, 5\%\}$, for Example 2.

The second example analysed in this paper is related again to the modified Helmholtz equation and contains a singularity at the origin O, which is caused by a sharp corner in the boundary, as well as the nature of the analytical potential solution corresponding to this problem, see Eqs. (11) and (37), for perturbed boundary potential measurements $u|_{\Gamma_D}$. The analytical and numerical fluxes on the boundaries EO and OA obtained in this case are shown in Figs. 10(a) and (b), respectively. Although not presented, it is worth mentioning that the numerical flux obtained on EO ∪ OA using the standard MFS ($n_S = 0$) exhibits very high oscillations in the neighbourhood of the singular point and hence it represents an inaccurate approximation for the analytical flux. The numerical potential solution and normal flux on the under-specified boundary BC, obtained using the regularized MFS+SST for various levels of noise added into $u|_{\Gamma_D}$, are illustrated in Figs. 10(c) and (d), respectively. The effect of the TRM and the MFS+SST algorithm on the accuracy of the numerical results in comparison with the LSM is clearly displayed in Table 3, which presents the relative RMS errors, $e_u(BC)$ and $e_q(BC)$, and the values for the corresponding optimal regularization parameter, λ_{opt}, obtained on the under-specified boundary BC using the LSM and TRM. From Figs. 10(c) and (d) and Table 3 we can conclude that the numerical results for the potential solution and normal flux on the under-specified boundary BC are also excellent approximations for their corresponding exact values and, in addition, they are convergent and stable with respect to decreasing the amount of noise added into the input boundary potential solution $u|_{\Gamma_D}$.

Table 3
The relative RMS errors, $e_u(BC)$ and $e_q(BC)$, and the values for the corresponding optimal regularization parameter, λ_{opt}, obtained using the LSM and TRM, $n_S = 5$ and various levels of noise added into the potential solution $u|_{\Gamma_D}$, namely $p_u \in \{1\%, 3\%, 5\%\}$, for Example 2.

Method	p_u (%)	e_u (BC)	e_q (BC)	λ_{opt}
LSM	1	0.13585×10^1	0.50453×10^2	–
	3	0.40755×10^1	0.15136×10^3	–
	5	0.67924×10^1	0.25226×10^3	–
TRM	1	0.54359×10^{-3}	0.48179×10^{-2}	1.0×10^{-4}
	3	0.91608×10^{-3}	0.54250×10^{-2}	1.0×10^{-3}
	5	0.20574×10^{-2}	0.15029×10^{-1}	1.0×10^{-3}

Consider now the singular inverse problem for the two-dimensional Helmholtz equation, as given by Example 3, with perturbed boundary potential solution on Γ_D. This singular Cauchy problem is actually the most severe one among the inverse problems investigated in this study, in the sense that the singularity at O is caused by all factors that may occur in such a situation, namely a sharp re-entrant corner and abrupt change in boundary conditions on the side DO ∪ OA (here $u|_{OA}$ and $q|_{DO}$ are prescribed), see Fig. 1(c), as well as the nature of the analytical potential solution corresponding to this problem, see Eqs. (12) and (38). Figs. 11(a) and (b) present the numerical solutions for the
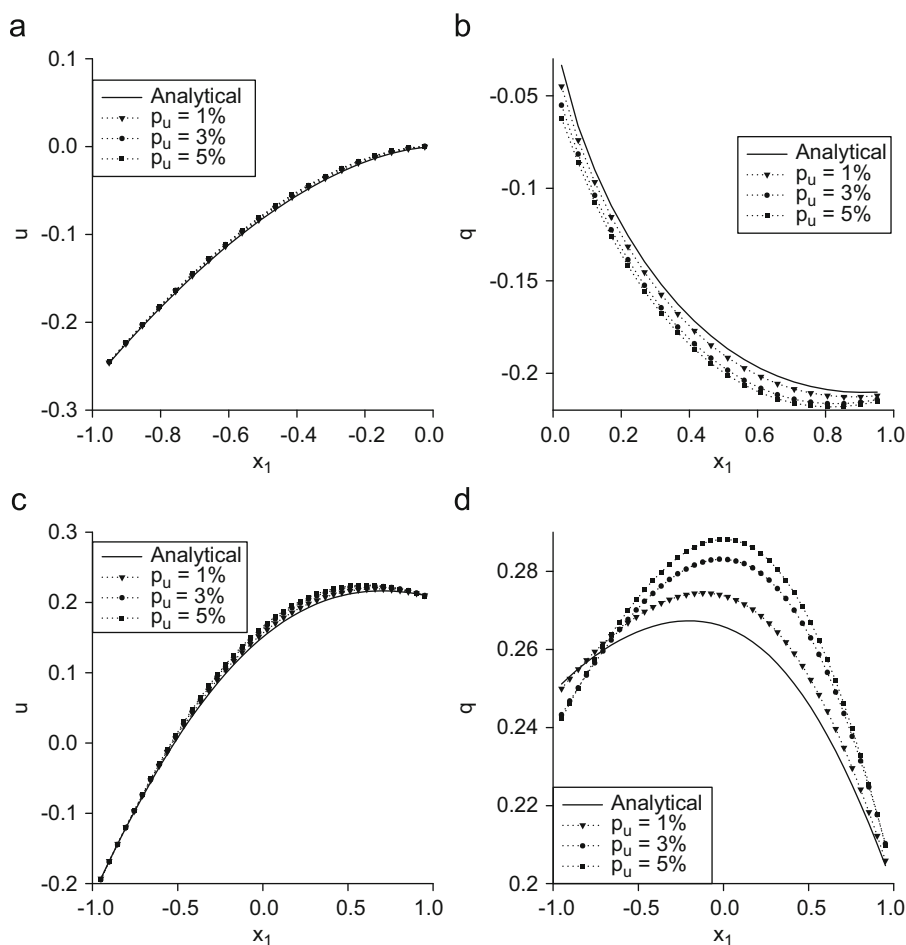
Fig. 11. Analytical and numerical solutions for (a) $u|_{DO}$ and (b) $q|_{OA}$, (c) $u|_{BC}$, and (d) $q|_{BC}$, obtained using the TRM, $n_S = 5$ and various levels of noise added into the Dirichlet data, $u|_{\Gamma_D}$, namely $p_u \in \{1\%, 3\%, 5\%\}$, for Example 3.

Table 4
The numerically retrieved values, $a_j^{(num)}$, for the flux intensity factors and the corresponding absolute errors, $Err(a_j)$, obtained using the TRM, $n_S = 5$ and various levels of noise added into the potential solution $u|_{\Gamma_D}$, namely $p_u \in \{1\%, 3\%, 5\%\}$, for Example 3.

p_u (%)	$a_1^{(num)}$	$Err(a_1)$	$a_2^{(num)}$	$Err(a_2)$	$a_3^{(num)}$	$Err(a_3)$	$a_4^{(num)}$	$Err(a_4)$
1	0.0048	0.48×10^{-2}	1.0142	0.14×10^{-1}	-1.5214	0.21×10^{-1}	1.0863	0.21×10^{0}
3	0.0086	0.86×10^{-2}	1.0411	0.41×10^{-1}	-1.5404	0.40×10^{-1}	0.5801	0.72×10^{0}
5	0.0116	0.12×10^{-1}	1.0463	0.46×10^{-1}	-1.5564	0.56×10^{-1}	0.4862	0.81×10^{0}

potential solution $u|_{DO}$ and normal flux $q|_{OA}$, respectively, retrieved by the TRM and various levels of noise added into $u|_{\Gamma_D}$, in comparison with their analytical counterparts, for Example 3. It can be seen from these figures that the numerical results for both the potential solution and the normal flux on the edges adjacent to the singularity point O are in very good agreement with their corresponding analytical values and being at the same time exempted from high and unbounded oscillations. Accurate, stable and convergent results have also been obtained for the unspecified potential solution $u|_{BC}$ and normal flux $q|_{BC}$ when the modified MFS described in Section 5, as can be observed form Figs. 11(c) and (d), respectively. However, the numerical normal fluxes $q|_{BC}$ are more inaccurate than the associated potential solutions $u|_{BC}$, as can be noticed by comparing Figs. 11(c) and (d), and this is a direct consequence of the

severity of the singular inverse problem given by Example 3. In addition, from these figures it can be concluded that both numerical potential solutions and normal fluxes on the under-specified boundary BC are convergent and stable with respect to decreasing p_u. Similar conclusions can be drawn from Table 4, which tabulates the numerical flux intensity factors, $a_j^{(num)}$, $j = 1, \ldots, 4$, and the corresponding absolute errors, $Err(a_j)$, $j = 1, \ldots, 4$, obtained using the TRM and various levels of noise added into the potential solution $u|_{\Gamma_D}$.

Overall, from the numerical results presented in this section it can be concluded that the MFS+SST proposed in Section 5, combined with the TRM and Hansen's L-curve criterion described in Section 6, is a very suitable method for solving inverse boundary value problems exhibiting singularities caused by the presence of sharp corners in the boundary of the solution domain

and/or abrupt changes in the boundary conditions, for two-dimensional Helmholtz-type equations with noisy boundary data. The numerical potential solutions and normal fluxes retrieved using this regularized MFS+SST are very good approximations for their analytical values on the entire boundary, they are exempted from oscillations in the neighbourhood of the singularity point and there is no need of further mesh refinement in the vicinity of the singularities.

8. Conclusions

In this study, the MFS was applied for solving, in an accurate and stable manner, inverse problems associated with two-dimensional Helmholtz-type equations in the presence of boundary singularities. The existence of such boundary singularities affect adversely the accuracy and convergence of standard numerical methods. Therefore, the MFS solutions to such problems and/or their corresponding derivatives, obtained by a direct inversion of the MFS system, may have unbounded values in the vicinity of the singularity. This difficulty was overcome by subtracting from the original MFS solution the corresponding singular potential solutions, as given by the asymptotic expansion of the potential solution near the singularity point, and at the same time employing the TRM, in conjunction with Hansen's L-curve method for choosing the optimal regularization parameter. Hence, in addition to the original MFS unknowns, new unknowns were introduced, namely the so-called flux intensity factors. Consequently, the original MFS system was extended by considering a number of additional equations which equals the number of flux intensity factors introduced and specifically imposes the type of singularity analysed in the vicinity of the singularity point. The proposed MFS+SST was implemented and analysed for singular inverse problems associated with both the Helmholtz and the modified Helmholtz equations in two-dimensional domains containing an edge crack or a V-notch, as well as an L-shaped domain.

From the numerical results presented in this paper, we can conclude that the advantages of the proposed method over other methods, such as mesh refinement in the neighbourhood of the singularity, the use of singular BEMs and/or FEMs etc., are the high accuracy which can be obtained even when employing a small number of collocation points and sources, and the simplicity of the computational scheme. A possible drawback of the present method is the difficulty in extending the method to deal with singularities in three-dimensional problems since such an extension is not straightforward. The extension of the current approach to inverse boundary value problems associated with two-dimensional isotropic linear elastic materials, as well as two-dimensional biharmonic equation, is currently under investigation.

References

[1] Chen JT, Wong FC. Dual formulation of multiple reciprocity method for the acoustic mode of a cavity with a thin partition. Journal of Sound and Vibration 1998;217:75–95.

[2] Kraus AD, Aziz A, Welty J. Extended surface heat transfer. New York: Wiley; 2001.

[3] Chen JT, Liang MT, Chen IL, Chyuan SW, Chen KH. Dual boundary element analysis of wave scattering from singularities. Wave Motion 1999;30:367–81.

[4] Huang C, Wu Z, Nevels RD. Edge diffraction in the vicinity of the tip of a composite wedge. IEEE Transactions on Geoscience and Remote Sensing 1993;31:1044–50.

[5] Barbone PA, Montgomery JM, Michael O, Harari I. Scattering by a hybrid asymptotic/finite element. Computer Methods in Applied Mechanics and Engineering 1998;164:141–56.

[6] Cai W, Lee HC, Oh HS. Coupling of spectral methods and the *p*-version for the finite element method for elliptic boundary value problems containing singularities. Journal of Computational Physics 1993;108:314–26.

[7] Lucas TR, Oh HS. The method of auxiliary mapping for the finite element solutions of elliptic problems containing singularities. Journal of Computational Physics 1993;108:327–42.

[8] Wu X, Han H. A finite-element method for Laplace- and Helmholtz-type boundary value problems with singularities. SIAM Journal on Numerical Analysis 1997;134:1037–50.

[9] Xu YS, Chen HM. Higher-order discretised boundary conditions at edges for TE waves. IEEE Proceedings—Microwave Antennas and Propagation 1999;146:342–8.

[10] Marin L, Lesnic D, Mantič V. Treatment of singularities in Helmholtz-type equations using the boundary element method. Journal of Sound and Vibration 2004;278:39–62.

[11] Li Z-C, Lu TT. Singularities and treatments of elliptic boundary value problems. Mathematical and Computer Modelling 2000;31:97–145.

[12] Mathon R, Johnston RL. The approximate solution of elliptic boundary value problems by fundamental solutions. SIAM Journal on Numerical Analysis 1977;14:638–50.

[13] Fairweather G, Karageorghis A. The method of fundamental solutions for elliptic boundary value problems. Advances in Computational Mathematics 1998;9:69–95.

[14] Golberg MA, Chen CS. The method of fundamental solutions for potential, Helmholtz and diffusion problems. In: Golberg MA, editor. Boundary integral methods: numerical and mathematical aspects. Boston: WIT Press and Computational Mechanics Publications; 1999. p. 105–76.

[15] Fairweather G, Karageorghis A, Martin PA. The method of fundamental solutions for scattering and radiation problems. Engineering Analysis with Boundary Elements 2003;27:759–69.

[16] Cho HA, Golberg MA, Muleshkov AS, Li X. Trefftz methods for time dependent partial differential equations. CMC: Computers, Materials & Continua 2004;1:1–37.

[17] Hon YC, Wei T. A fundamental solution method for inverse heat conduction problems. Engineering Analysis with Boundary Elements 2004;28:489–95.

[18] Mera NS. The method of fundamental solutions for the backward heat conduction problem. Inverse Problems in Science and Engineering 2005;13:79–98.

[19] Marin L, Lesnic D. The method of fundamental solutions for the Cauchy problem in two-dimensional linear elasticity. International Journal of Solids and Structures 2004;41:3425–38.

[20] Marin L. A meshless method for solving the Cauchy problem in three-dimensional elastostatics. Computers & Mathematics with Applications 2005;50:73–92.

[21] Marin L. Numerical solutions of the Cauchy problem for steady-state heat transfer in two-dimensional functionally graded materials. International Journal of Solids and Structures 2005;42:4338–51.

[22] Marin L, Lesnic D. The method of fundamental solutions for the Cauchy problem associated with two-dimensional Helmholtz-type equations. Computers & Structures 2005;83:267–78.

[23] Marin L. A meshless method for the numerical solution of the Cauchy problem associated with three-dimensional Helmholtz-type equations. Applied Mathematics and Computation 2005;165:355–74.

[24] Jin B, Zheng Y. A meshless method for some inverse problems associated with the Helmholtz equation. Computer Methods in Applied Mechanics and Engineering 2006;195:2270–80.

[25] Jin B, Marin L. The method of fundamental solutions for inverse source problems associated with the steady-state heat conduction. International Journal for Numerical Methods in Engineering 2007;69:1570–89.

[26] Karageorghis A. Modified methods of fundamental solutions for harmonic and biharmonic problems with boundary singularities. Numerical Methods for Partial Differential Equations 1992;8:1–19.

[27] Poullikkas A, Karageorghis A, Georgiou G. Methods of fundamental solutions for harmonic and biharmonic boundary value problems. Computational Mechanics 1998;21:416–23.

[28] Karageorghis A, Poullikkas A, Berger JR. Stress intensity factor computation using the method of fundamental solutions. Computational Mechanics 2006;37:445–54.

[29] Berger JR, Karageorghis A, Martin PA. Stress intensity factor computation using the method of fundamental solutions: mixed mode problems. International Journal for Numerical Methods in Engineering 2007;69:469–83.

[30] Marin L. Stable MFS solution to singular direct and inverse problems associated with the Laplace equation subjected to noisy data. CMES: Computer Modeling in Engineering & Sciences 2008;37:203–42.

[31] Marin L. Treatment of singularities in the method of fundamental solutions for two-dimensional Helmholtz-type equations. Applied Mathematical Modelling, 2009 [in press], doi:10.1016/j.apm.2009.09.009.

[32] Portela A, Aliabadi MH, Rooke DP. Dual boundary element analysis of cracked plates: singularity subtraction technique. International Journal Fracture 1992;55:17–28.

[33] Hadamard J. Lectures on Cauchy problem in linear partial differential equations. New Haven: Yale University Press; 1923.

[34] Gorzelańczyk P, Kołodziej A. Some remarks concerning the shape of the shape contour with application of the method of fundamental solutions to elastic torsion of prismatic rods. Engineering Analysis with Boundary Elements 2008;32:64–75.

[35] Tikhonov AN, Arsenin VY. Methods for solving ill-posed problems. Moscow: Nauka; 1986.

[36] Morozov VA. On the solution of functional equations by the method of regularization. Soviet Mathematical Doklady 1966;7:414–7.

[37] Wahba G. Practical approximate solutions to linear operator equations when the data are noisy. SIAM Journal on Numerical Analysis 1977;14:651–67.

[38] Hansen PC. Rank-deficient and discrete ill-posed problems: numerical aspects of linear inversion. Philadelphia: SIAM; 1998.